
# Charge to spin conversion in van der Waals metal NbSe<inf>2</inf>

Applied Physics Letters ARTICLE scitation.org/journal/apl

# Charge to spin conversion in van der Waals metal $NbSe_2$

Cite as: Appl. Phys. Lett. **121**, 242404 (2022); doi: 10.1063/5.0121577
Submitted: 18 August 2022 · Accepted: 30 November 2022 ·
Published Online: 13 December 2022



Anamul Md. Hoque,[1] Bing Zhao,[1] Dmitrii Khokhriakov,[1] Prasanta Muduli,[2] and Saroj P. Dash[1,3,a)]

## AFFILIATIONS

[1]Department of Microtechnology and Nanoscience, Chalmers University of Technology, SE-41296 Göteborg, Sweden
[2]Department of Physics, Indian Institute of Technology Madras, Chennai 600036, India
[3]Graphene Center, Chalmers University of Technology, SE-41296 Göteborg, Sweden

[a)]Author to whom correspondence should be addressed: saroj.dash@chalmers.se

## ABSTRACT

Quantum materials with a large charge current-induced spin polarization are promising for next-generation all-electrical spintronic science and technology. Van der Waals metals with high spin–orbit coupling and spin textures have attracted significant attention for an efficient charge-to-spin conversion process. Here, we demonstrate the electrical generation of spin polarization in $NbSe_2$ up to room temperature. Characterization of $NbSe_2$ shows superconducting transition temperature, $T_c \sim 7$ K. To probe the current-induced spin polarization in $NbSe_2$, we used a graphene-based non-local spin-valve device, where the spin-polarization in $NbSe_2$ is efficiently injected and detected using non-local spin-switch and Hanle spin precession measurements. A significantly higher charge-spin conversion in $NbSe_2$ is observed at a lower temperature. Systematic measurements provide the possible origins of the spin polarization to be predominantly due to the spin Hall effect or Rashba–Edelstein effect in $NbSe_2$, considering different symmetry-allowed charge-spin conversion processes.



Two-dimensional (2D) materials and their van der Waals (vdW) heterostructures have become attractive platforms to explore numerous physical phenomena, primarily associated with spin–orbit coupling (SOC), exotic superconductivity, and magnetism for next-generation electronic devices.[1,2] While graphene is ideal for spin interconnect[3] in spin logic applications[4] and 2D magnets as spin injectors,[5] the 2D transition metal dichalcogenides (TMDCs) are ideal hosts for realizing spin-polarized electronic states due to the high SOC accompanied by broken symmetries in the crystal structure.[6,7] Recently, vdW materials have paved the way for utilizing various charge-to-spin interconversion (CSC) processes.[6,8] For example, charge-to-spin interconversion and spin–orbit torque (SOT) effects are observed in semimetals such as $WTe_2$, $MoTe_2$, and $NbSe_2$ up to room temperature.[9–14] Furthermore, the 2D materials can be fabricated in vdW heterostructures with atomically clean interfaces without adulterating their distinctive electronic properties that provide routes for band structure engineering and proximity-induced SOC.[15] For instance, heterostructures of graphene with 2D materials have shown unprecedented gate-tunable CSC processes and spin textures.[13,16–21]

It is known that 2H-$NbSe_2$ is a vdW layered metallic TMDC with superconducting (SC) behavior below a critical temperature $T_c \approx 7$ K.[22] It is expected that the CSC effects can be enhanced in the SC state mediated by quasiparticles with higher spin lifetimes.[2,23] Interestingly, $NbSe_2$ in the normal state also has enormous prospects in the CSC process, triggered by high SOC of the Nb 4*d* orbital and breaking of symmetries with higher electrical conductivities than semiconductive and semimetallic TMDCs.[9] $NbSe_2$ also exhibits Ising-type SOC similar to the intrinsic Zeeman field, which results in unconventional spin textures.[24] Recently, $NbSe_2$/Permalloy structures demonstrated a large anti-damping torque, which is attributed to strain-induced symmetry breaking.[9] Furthermore, spin- and angle-resolved photoemission spectroscopy (ARPES) also reveals that the electronic band structure of $NbSe_2$ in the normal state hosts a strong momentum-dependent spin polarization at Fermi level.[25] Such fascinating spin-dependent electronic properties in $NbSe_2$ are highly desirable to create current-induced spin polarization.

Here, we demonstrate the electronic generation of spin polarization in $NbSe_2$ up to room temperature owing to the efficient CSC process. The engendered spin polarization in $NbSe_2$ is efficiently injected into the graphene spin-channel in the vdW heterostructure spin-valve device and detected by a ferromagnet (FM) using non-local (NL) spin-switch and Hanle spin-precession measurements. A significantly higher CSC signal in $NbSe_2$ is observed at a lower temperature in the non-superconducting regime. These findings demonstrate $NbSe_2$ to be

a metallic spin source up to room temperature, which can be pivotal for future energy-efficient all-electric spin-based technologies.[26,27]

To detect the CSC properties in $NbSe_2$, we fabricated $NbSe_2$-graphene vdW heterostructure devices. We used chemical vapor deposited (CVD) graphene as a spin channel material, due to its excellent spin transport properties arising from low SOC and hyperfine interactions,[28,29] with demonstration of multifunctional spin logic operations.[4] Most interestingly, it was demonstrated that graphene can make a very good vdW heterostructure with other 2D materials.[30] Figure 1(a) presents the schematic of the $NbSe_2$-graphene vdW heterostructure device along with ferromagnetic (FM) contacts to characterize the spin transport properties in the heterostructure (see the Methods in the supplementary material for details). A scanning electron microscope (SEM) image of a fabricated device consisting of CVD graphene, multilayer $NbSe_2$ flake, and multiple FM contacts is shown in Fig. 1(b). An optical micrograph and atomic force microscope (AFM) image of the corresponding device have been shown in supplementary material Fig. S1. The interface resistance between $NbSe_2$-graphene is found to be 50 Ω, the FM contact resistance is 12 kΩ, and the field-effect mobility ($\mu$) of the graphene channel is $\approx$2000 $cm^2\,V^{-1}\,s^{-1}$ (see supplementary material Fig. S2).

As a high SOC material, $NbSe_2$ can give rise to current-induced in-plane (y-axis) spin polarization via conventional spin Hall effect [shown in Fig. 1(c)], where charge current ($I_c$) along the x-axis creates a transverse spin current ($I_s$) along the z-axis.[12,14] Furthermore, high SOC in $NbSe_2$ crystal along with structure inversion asymmetry (SIA) in the layered $NbSe_2$-graphene interface can result in Rashba spin splitting in the band structure with helical spin texture with opposite spin-subbands, as shown in Fig. 1(d). Upon application of an electric field (E), the charge current can shift the helical Fermi surface in the k-space and create net spin polarization via the Rashba–Edelstein effect. The created spin polarization in $NbSe_2$ can be injected into a graphene spin channel in vdW heterostructure and detected by NL measurement geometry to realize a pure spin signal.

At first, high-quality crystal structures of the materials were ensured by Raman spectroscopy. The Raman spectrum of single-layer CVD graphene (top panel) and exfoliated multilayer $NbSe_2$ (bottom panel) using 638 nm LASER have been presented in Fig. 2(a). The Raman spectra of graphene confirm high-quality graphene crystal since almost no defect-induced D peak is observed. Furthermore, the higher intensity of the 2D peak at 2645 $cm^{-1}$ than that of the G peak at 1590 $cm^{-1}$ indicates the growth of single-layer graphene.[31] In the case of $NbSe_2$, the characteristic $A_{1g}$ peak for multilayer 2H-$NbSe_2$ is observed at 230 $cm^{-1}$.[32]

We started with investigating the superconducting properties of exfoliated multilayer $NbSe_2$ flake by measuring the temperature dependence of longitudinal resistance, as shown in Fig. 2(b). The device picture and measurement geometry are shown in the insets of Fig. 2(b). We used 1$\mu$A of DC bias current, and the superconducting critical temperature ($T_c$) in this flake is found to be 6.8 K.

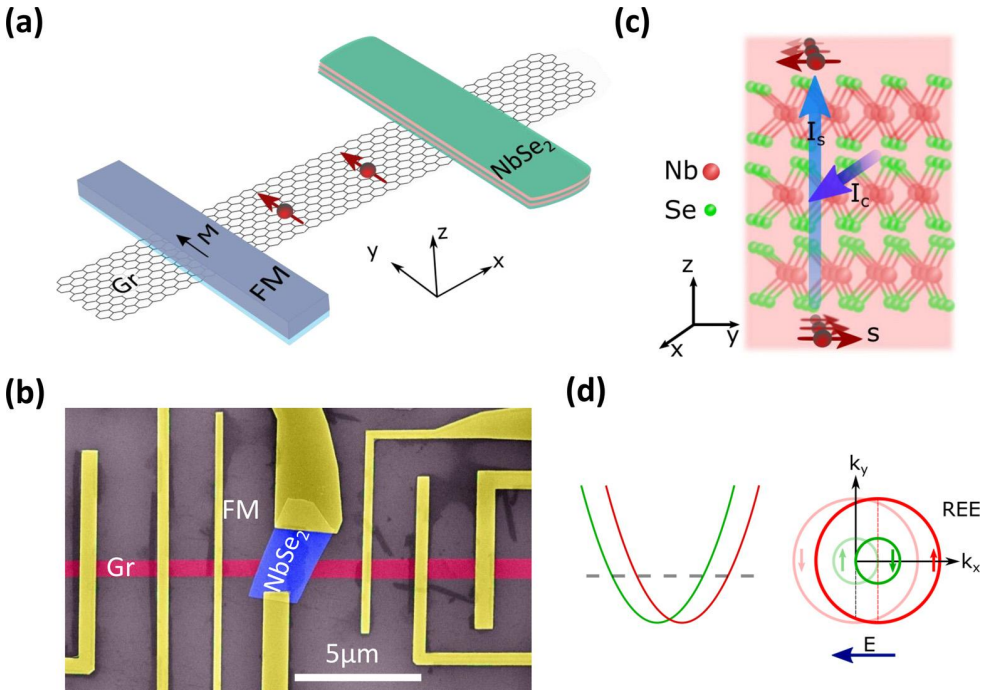


**FIG. 1.** The device design of $NbSe_2$-graphene heterostructure. (a) Schematic of $NbSe_2$-graphene heterostructure, where $NbSe_2$ creates non-equilibrium spin polarization and injects spin-polarized electrons into graphene spin-channel, which is detected by an FM ($TiO_2$/Co) contact in non-local measurement geometry. (b) Colored scanning electron microscope (SEM) image of a fabricated device consisting of CVD graphene, multilayer $NbSe_2$ flake (blue), and multiple FM contacts (yellow) to characterize spin transport properties. The scale bar is 5 $\mu$m. (c) Schematic illustration of charge to spin conversion process due to conventional spin Hall effect in $NbSe_2$, where charge current ($I_c$) engenders a transverse spin current ($I_s$). (d) Schematics of the energy dispersion (left) and the Fermi surface (right) of a high spin-orbit coupling interface with Rashba spin-orbit coupling. The charge current(Ic) or Electric Field (E) shifts the Fermi contours from equilibrium and produces nonequilibrium spin accumulation via the Rashba–Edelstein effect.

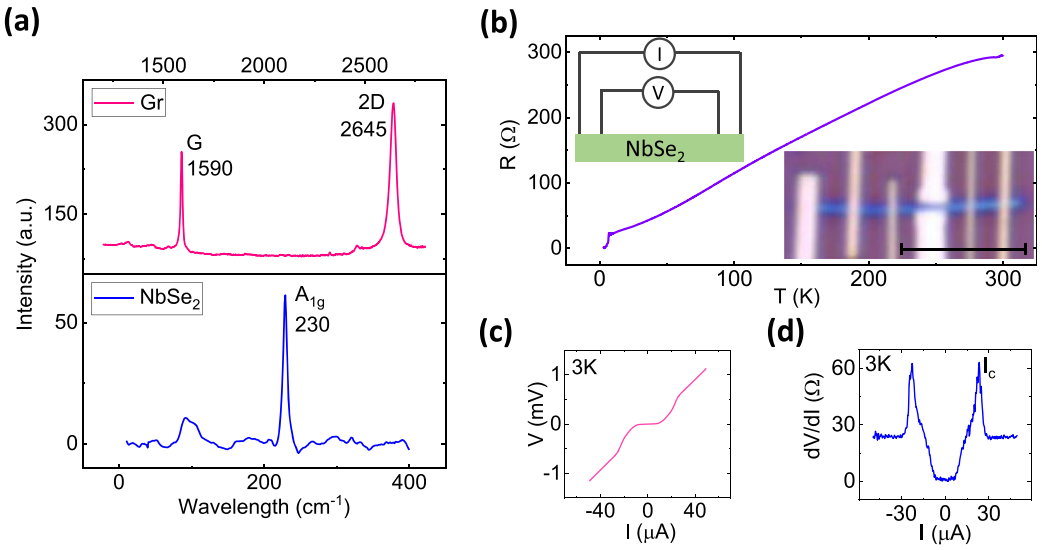


**FIG. 2.** Materials characteristics of $NbSe_2$ and graphene. (a) Raman spectrum of single-layer CVD graphene (top panel) and exfoliated multilayer $NbSe_2$ (bottom panel) using 638 nm LASER. (b) Temperature dependence of the longitudinal resistance of multilayer $NbSe_2$ flake, where superconducting critical temperature ($T_c$) around 6.8 K is evident. Insets are the four-terminal measurement geometry (top) and device picture (bottom) along with a scale bar of 5 $\mu$m. (c) and (d) The four-probe IV measurements and corresponding differential resistance as a function of the bias current in the multilayer $NbSe_2$ flake at 3 K.

The IV measurement with DC bias current and corresponding differential resistance (dV/dI) as a function of the bias current at 3 K for the $NbSe_2$ flake are shown in Figs. 2(c) and 2(d), respectively. The nonlinear IV is due to superconductive properties in $NbSe_2$, and from the dV/dI plot, we can estimate the critical current density, $J_{c,\,NbSe2} = 0.7 \times 10^6$ A/cm$^2$ for the multilayer $NbSe_2$ at 3 K, consistent with the recent study.[33] The room temperature IV measurement [supplementary material Figs. S3(b) and S3(c)] is in agreement with the metallic properties of $NbSe_2$. Raman spectroscopies together with the presence of superconducting transition in $NbSe_2$ confirm good-quality materials are used in the heterostructure.

To investigate the CSC effect in $NbSe_2$, a charge current is applied in a multilayer $NbSe_2$ flake to create a non-equilibrium spin polarization on its surface. The spins are injected into the graphene channel and finally detected by an FM contact in NL measurement geometry. Figure 3(a) shows a schematic illustration of the measurement geometry used to detect the CSC effect in $NbSe_2$ along with the axis orientation and corresponding spin polarization ($\hat{s}$), charge current ($I_c$), and spin current ($I_s$) directions. According to our measurement geometry in Fig. 3(a) by considering conventional SHE in $NbSe_2$, a charge current along x-axis can create an out-of-plane (z-axis) spin current, which renders spin polarization along y-axis. It is worth mentioning that the spin diffusion current in graphene spin channel is along x-axis in our measurement geometry with spin orientation toward y-axis after spin polarization is created in $NbSe_2$ and injected into graphene. In our experiments, we measure the NL voltage at the FM contact (left nearest contact to the $NbSe_2$ flake, shown in Fig. 1(b) by applying varying magnetic fields along the $B_y$ and $B_z$ directions). A varying magnetic field along the magnetic easy axis (y-axis) switches the magnetization of the FM contact and renders a switching signal that detects non-equilibrium in-plane spin in graphene injected from the $NbSe_2$ flake. The spin-switch signal presented in Fig. 3(b) is measured

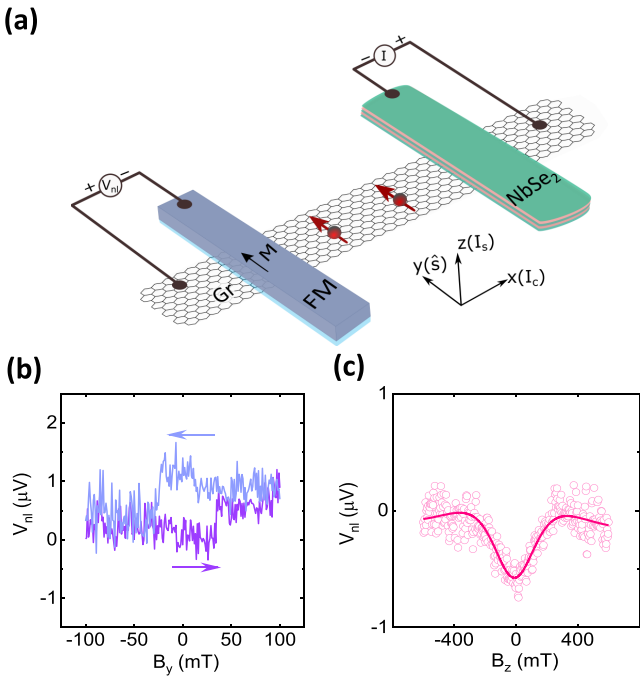


**FIG. 3.** Charge-spin conversion in $NbSe_2$ at room temperature. (a) Schematic illustration of non-local measurement geometry to detect the charge-spin conversion effect in $NbSe_2$ by injecting spin current into the graphene spin channel. (b) and (c) The spin-switch and Hanle spin precession measurements for spin injection from $NbSe_2$ with $B_y$ and $B_z$ sweeps, respectively. For spin-switch experiments, the up and down magnetic sweep directions are indicated by arrows. The Hanle data are fitted using Eq. (S1). A linear background is subtracted from the data.

with I = 400 $\mu$A at $V_g = -40$ V. The amplitude of the signal estimated from the change in NL resistance corresponding to the opposite magnetization of the FM contact is about $\Delta R_{nl} = 1.77 \pm 0.6$ m$\Omega$.

Furthermore, an out-of-plane varying magnetic field ($B_z$) in our measurement geometry should render a Hanle spin precession signal, which unequivocally confirms the CSC process in the $NbSe_2$ and spin transport in the graphene spin channel. Figure 3(c) shows the manifested Hanle spin signal measured with I = +420 $\mu$A and $V_g = -40$ V while injecting spin from $NbSe_2$ into the graphene channel along with the fitting to Eq. (S1). We have estimated the spin lifetime, $\tau_s = 23 \pm 6$ ps, and spin diffusion length, $\lambda_s = \sqrt{\tau_s D_s} = 0.65 \pm 0.05$ $\mu$m, considering the channel length L = 2.4 $\mu$m (distance between the center of the $NbSe_2$ flake to the center of the detector FM electrode). Moreover, the spin transport in the pristine CVD graphene is shown in supplementary material Fig. S4, where spin lifetime is estimated to be around 150 ps. To mention, we observe variations in spin lifetime in different CVD graphene channels in the range of 100–400 ps. In $NbSe_2$-graphene heterostructure, the lower $\tau_s$ in graphene spin channel after spin is injected from $NbSe_2$ can be attributed to the influence of long-range disorders, lattice deformation, and extrinsic interstitials in the graphene crystal that acts as spin-defect centers. These imperfections might be introduced during processing CVD graphene, $NbSe_2$ transfer, and device fabrication processes. Additionally, spin absorption by $NbSe_2$ can also give rise to lower $\tau_s$ because of the transparent $NbSe_2$–graphene interface.[34] Interestingly, only a symmetric Hanle component is observed although the $NbSe_2$ flake in our device is at an angle to the graphene spin channel.[35] Furthermore, any contribution of the spin injection from the FM contact on $NbSe_2$ can be eliminated from the spin switch signal because the influence of the FM magnetization would have manifested a typical spin valve signal [as presented in Fig. S4(a)] with double spin-valve switching while sweeping $B_y$. If any spin component other than the y-axis were present, the Hanle measurement would have rendered an anti-symmetric component, which was not observed, presumably due to the small efficiency of SHE in other directions. In addition, the Hanle measurement rules out any effect of stray fields from the detector FM contacts on the manifested CSC signals since the stray Hall effect would have rendered a linear Hall signal for an out-of-plane field ($B_\perp$).[36]

Next, we estimated the spin polarization of $NbSe_2$ is about $P_{NbSe2} = 1 \pm 0.3\%$, assuming the spin polarization of FM contact on bare CVD graphene is $P_{Co} = 1.5 \pm 0.6\%$ (see supplementary material Note 1). This estimated spin-polarization accounts for the creation of spin polarized carriers in $NbSe_2$ along the y-axis and injected into the graphene channel through the vdW gap. The efficiency of the CSC process due to spin Hall effect in $NbSe_2$ can be characterized by the spin Hall angle ($\theta_{SH} \propto J_s/J_c$), and by using a simple model (as discussed in supplementary material Note 1), we found the $\theta_{SH}$ of $NbSe_2$ varies approximately from $0.68 \pm 0.15$ to $0.30 \pm 0.06$ by assuming the variation of spin diffusion length in $NbSe_2$, $\lambda_{NbSe2} = 5$–40 nm [see Fig. S5(a) and supplementary material Note 2].[12,14,37,38] This estimation of $\theta_{SH}$ is consistent with the recently reported theoretical study, where $\theta_{SH}$ in $NbSe_2$ is predicted to be $\approx 0.5$ by light irradiation.[39] Note that the spin diffusion length ($\lambda_{NbSe2}$) in $NbSe_2$ is not experimentally reported yet. We also analytically calculated the length scale, $\theta_{SH}$. $\lambda_{NbSe2} \sim 5$–13 nm associated with the CSC in $NbSe_2$ [supplementary material Fig. S5(b)], which is comparable to the recently reported length scale in layered TMDCs, e.g., 1.15 nm in $MoTe_2$[12].

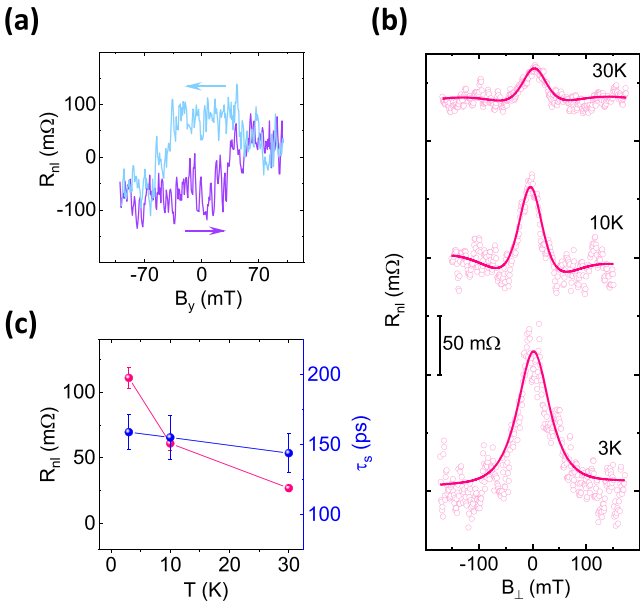


**FIG. 4.** Temperature dependence of the charge-spin conversion effect in $NbSe_2$. (a) Spin-switch signal for the charge-spin conversion effect in $NbSe_2$ (Dev. 2) resulting in spin injection from $NbSe_2$ into graphene at 3 K. (b) Hanle spin precession measurements along with the fitting to Eq. S1 (solid line). Measurements were performed in Dev 2 in a bias current range of 200–500 $\mu$A and at $V_g = -40$ V. A linear background is subtracted from the data and shifted along the y-axis for clear visualization. (c) The magnitude of the Hanle spin signal $\Delta R_{nl}$ and extracted spin lifetime ($\tau_s$) at different temperatures.

We restrict our calculation by assuming $\lambda_{NbSe2} = 5$–40 nm, comparable to spin diffusion length of other TMDCs, e.g., $\lambda_{WTe2} = 8$ nm, and to get reasonable $\theta_{SH}$.[14] Another plausible origin of the measured CSC signal could be the Rashba–Edelstein effect (REE) due to Rashba spin-split bands in $NbSe_2$ and its proximity effect in the $NbSe_2$-graphene heterostructure region.[7] The characteristic efficiency parameter ($\alpha_{RE}$) of the REE is calculated (supplementary material Note 2) to be $5.3 \pm 1.8\%$, which is consistent with the recent studies on 2D material heterostructures.[12,13,17,18,40] Considering assumptions made in the model to evaluate the spin Hall angle, we obtain a very rough estimation of $\theta_{SH}$ in $NbSe_2$, and further theoretical calculations are needed to provide more accurate values of these parameters.

We measured the temperature dependence of the CSC process in $NbSe_2$ to observe the evolution of spin polarization in $NbSe_2$ with temperature in Dev2 [Fig. S1(d)]. Figure 4(a) shows the NL spin-switch signal arising due to the CSC effect in $NbSe_2$ and subsequent spin injection into graphene at 3 K. The magnitude of the CSC signal is found to be $\Delta R_{nl} \approx 106 \pm 27$ m$\Omega$. Next, we measured the Hanle spin precession signal above and below $T_c$ of $NbSe_2$ to validate the manifested spin-switch signal is a spin-related phenomenon. Figure 4(b) shows the Hanle signals along with the fitting to Eq. (S1). The magnitude of the Hanle spin signal, $\Delta R_{nl}$, and extracted spin lifetime $\tau_s$ at different temperatures (3–30 K) have been shown in Fig. 4(c). Interestingly, we found that the $\Delta R_{nl}$ increases drastically below

$T_c$, but $\tau_s$ remains mostly unchanged around 150 ps, below and above $T_c$, because spin transport parameters of graphene are known to be weakly dependent on temperature.[11,29] We would like to note that, as $\tau_s$ remains unchanged, the larger $\Delta R_{nl}$ can be attributed to more efficient CSC conversion effect below $T_c$. However, the increase in CSC signal with decreasing temperature could also be due to the decrease in $NbSe_2$ resistivity ($\rho_{NbSe2}$) and conductivity mismatch between $NbSe_2$ and graphene interface.

It is expected that the quasiparticle mediated CSC process is enhanced near the superconducting state of the corresponding material.[23] Although we observed CSC signal in $NbSe_2$ at 3 K (below Tc ~ 7 K), we would also like to mention that the $NbSe_2$ flake is not in the superconducting state in our CSC experiments as the applied bias current density ($\sim 4 \times 10^6$ A/cm$^2$) is much higher than the critical current density ($\sim 0.7 \times 10^6$ A/cm$^2$ at 3 K). We optimized the bias current magnitude to maximize the CSC signal at different temperatures that surmount the noise level of the signals, which vary due to the conductivity mismatch of the $NbSe_2$ and detector FM contact with the graphene spin channel.

Here, we discuss possible origins that can give rise to the manifested CSC signal in $NbSe_2$. First and foremost, the NL spin-switch with varying in-plane $B_y$ field and Hanle spin-precession measurements with changing out-of-plane field $B_z$ confirm that the detected signals are due to the in-plane (y-axis) spin-polarized current that is created in $NbSe_2$ and injected into graphene. We can rule out the spin polarization generation via the proximity-induced spin Hall effect (SHE) because this effect would have resulted in an out-of-plane spin polarization ($s_z$) in the heterostructure region, which is not observed.[41] In addition, the proximity-induced Rashba–Edelstein (REE) effect in graphene from $NbSe_2$ should have rendered the opposite sign of the measured CSC signal for the p- and n-doped regimes.[16,18,40] However, we observed CSC signal only in the p-doped regime of graphene with a high negative gate voltage, most likely due to the conductivity mismatch issues of the graphene channel with $NbSe_2$ and FM contacts in the n-doped regime of graphene.[19,21,42] Hence, proximity-induced REE can neither be ruled out nor be claimed to be the origin of the observed CSC signal with our measurements. Furthermore, the unconventional CSC process, which is recently reported in multilayer TMDCs ($WTe_2$ and $MoTe_2$), cannot also be disregarded in $NbSe_2$ since it is a layered material with structural inversion asymmetry in the crystal structure that can be further enhanced by the induced strain at the vdW heterostructure device geometry.[11,12] Finally, considering the symmetry principle,[12] spin polarization direction (s) is set perpendicular to the applied charge current ($I_c$) and spin current ($I_s$) direction; the SHE and REE in $NbSe_2$ most likely merge or independently produce the observed CSC signal in $NbSe_2$. In future, the measurements of the CSC and inverse CSC (spin-to-charge conversion) processes in $NbSe_2$ with different device configurations and measurement geometries with different thicknesses and their correlation with properties in the superconducting state can be interesting. To be noted, during the review process of our manuscript, multidirectional spin-to-charge conversion in graphene/$NbSe_2$ van der Waals heterostructures has been reported.[43]

In summary, we demonstrated CSC in the normal metallic state of $NbSe_2$ up to room temperature. The engendered spin polarization can be injected into the graphene channel and detected in non-local measurement geometry via spin-switch and Hanle spin precession measurements. A higher CSC signal in $NbSe_2$ is detected at a lower temperature, however, in its non-superconducting state because of the requirement of a higher bias current than the critical current of $NbSe_2$ for the observation of spin signals. Systematic measurements of the spin-switch and Hanle signals reveal that the possible origins of the in-plane spin polarization are predominantly due to the spin Hall effect or the Rashba–Edelstein effect in $NbSe_2$ considering different symmetry-permitted CSC processes. Such features of current-induced spin polarization in $NbSe_2$ have promising potentials to be used as a non-magnetic spin source in future all-electric spintronic devices and spin–orbit technologies. Furthermore, the realization of CSC in superconducting quantum materials with high SOC strength can enhance the spintronic device performance by generating a larger spin current with a longer spin lifetime.[2]

See the supplementary material for the details about the device fabrication, characterization, and estimation of charge-spin conversion.

The authors acknowledge financial support from the EU Graphene Flagship (Core 3, No. 881603), the Swedish Research Council VR project grants (No. 2021-04821), the 2D TECH VINNOVA competence center (No. 2019-00068), FLAG-ERA Project 2DSOTECH (VR No. 2021-05925), Graphene center, EI Nano, and AoA Materials and AoA Energy programs at Chalmers University of Technology. We acknowledge the help of staff at the Quantum Device Physics and Nanofabrication laboratory in our MC2 department at Chalmers. Devices were fabricated at the Nanofabrication Laboratory, Myfab, MC2, Chalmers.

## AUTHOR DECLARATIONS

### Conflict of Interest

The authors have no conflicts to disclose.

### Author Contributions

**Anamul Md Hoque:** Conceptualization (lead); Data curation (lead); Formal analysis (equal); Investigation (lead); Validation (equal); Visualization (equal); Writing – original draft (equal); Writing – review & editing (equal). **Bing Zhao:** Data curation (lead); Formal analysis (supporting); Investigation (supporting); Validation (equal); Visualization (supporting); Writing – original draft (equal); Writing – review & editing (equal). **Dmitrii Khokhriakov:** Formal analysis (supporting); Investigation (supporting); Methodology (supporting); Writing – original draft (supporting); Writing – review & editing (supporting). **Prasanta Kumar Muduli:** Formal analysis (supporting); Investigation (supporting); Visualization (supporting); Writing – original draft (supporting); Writing – review & editing (equal). **Saroj Prasad Dash:** Conceptualization (lead); Formal analysis (equal); Funding acquisition (lead); Investigation (equal); Methodology (supporting); Project administration (lead); Supervision (lead); Visualization (equal); Writing – review & editing (equal).

## DATA AVAILABILITY

The data that support the findings of this study are available from the corresponding author upon reasonable request.